RESEARCH ARTICLE

ADVANCED FUNCTIONAL MATERIALS
www.afm-journal.de

Alginate-Sludge Derived Biochar-Calcium Hydrogel for Phosphate Removal and Slow-Release Fertilizer: A Sustainable and Multifunctional Solution

*Yu Zhang, Baile Wu, Haoran Dong, Xiaohong Guan, and Irene M. C. Lo**

Phosphorus (P) pollution and depletion pose significant environmental and agricultural challenges. In this study, a multifunctional alginate-biochar-calcium (ABC) hydrogel for efficient phosphate removal and slow-release fertilization is developed. The hydrogel is synthesized by pyrolyzing biological sewage sludge to produce biochar, followed by calcium chloride modification and cross-linking with sodium alginate. The ABC-hydrogel achieves a high phosphate adsorption capacity, with maximum adsorption of 252.15 mg g^{-1}, and enables controlled phosphate release, with 48% gradually released over 37 days, supporting sustained plant growth. Pot experiments demonstrate its agricultural benefits, with the P-loaded hydrogel enhancing the wet weight of lettuce by 110% compared to the control group. Additionally, the treatment methods, including pyrolysis, calcium modification, and crosslinking in hydrogel, significantly reduce the ecological risk of heavy metals in biological sewage sludge, lowering the ecological risk index (ERI) from 533.13 to 5.79, effectively transforming sludge from waste into a safe and valuable resource for agricultural and environmental applications. With a water absorption capacity of 439.22%, the hydrogel improves soil moisture retention, making it particularly beneficial for drought-prone regions. This work significantly contributes to sustainable phosphorus management by converting waste sludge into a valuable resource, offering promising applications in agriculture, phosphate removal, and waste reutilization.

1. Introduction

Phosphorus is a crucial nutrient for the growth of plants and is essential in agricultural production. However, the growing global demand for phosphorus, coupled with the rapid depletion of accessible phosphate rock reserves has raised concerns about the future sustainability of phosphorus supply.[1] Simultaneously, phosphorus pollution, primarily resulting from agricultural runoff, wastewater discharge, and industrial effluent, has become a significant environmental issue.[2] Excessive phosphorus in aquatic environments promotes eutrophication, leading to harmful algal blooms that disrupt aquatic ecosystems and threaten water biodiversity.[3–5] These adverse effects, particularly in lakes, rivers, and coastal zones, highlight the urgent need for effective phosphorus management strategies.

Current methods for phosphorus removal from wastewater include chemical precipitation, biological treatment, and adsorption. Among these, adsorption is increasingly recognized as a promising

Y. Zhang, I. M. C. Lo
Department of Civil and Environmental Engineering
The Hong Kong University of Science and Technology
Hong Kong 511453, China
E-mail: cemclo@ust.hk

B. Wu
School of Biological
Earth and Environmental Sciences
Environmental Research Institute
University College Cork
Cork T12 K8AF, Ireland

H. Dong
College of Environmental Science and Engineering
Hunan University
Changsha, Hunan 410082, China

X. Guan
School of Ecological and Environmental Sciences
East China Normal University
Shanghai 200241, China

I. M. C. Lo
Institute for Advanced Study
The Hong Kong University of Science and Technology
Hong Kong 511453, China

The ORCID identification number(s) for the author(s) of this article can be found under https://doi.org/10.1002/adfm.202510234

DOI: 10.1002/adfm.202510234

approach due to its operational simplicity, cost-effectiveness, and efficiency.[6] A variety of adsorbents have been explored for phosphorus removal, including activated carbon, mineral clays, polymers, and biochar. Biochar, in particular, has gained attention for its ability to adsorb phosphorus due to its porous structure, abundant functional groups, and high availability from diverse waste sources.[7–9] Depending on the feedstock and pyrolysis conditions, biochar can achieve a specific surface area of up to 1800 $m^2 g^{-1}$, contributing to its adsorption capability.[10] Biochar feedstock plays a crucial role in determining its adsorption properties. Common feedstocks for biochar include agricultural residues,[8] wood,[9] and sludge.[7] Biochar derived from sewage sludge, a major waste product from wastewater treatment, has shown significant promise for phosphorus adsorption due to its metal content (e.g., Ca, Mg, and Al), which enhances its phosphate retention capacity.[11,12]

Despite its advantages, the use of biochar for phosphorus adsorption faces a number of challenges, particularly in terms of its safe reuse and separation from water.[13,14] Sewage sludge often contains high concentrations of heavy metals, posing environmental and health risks if not properly managed.[15] The conventional treatment method for sludge by landfilling fails to address this issue. Furthermore, biochar is typically used in a fine powder form, making it difficult to separate from water, which significantly hinders its practical applications and reuse. As a result, there is a pressing need to develop biochar-based composite materials that can overcome these limitations and provide a sustainable solution for phosphorus removal and recovery.

Additionally, the use of traditional phosphate fertilizers has exposed several inefficiencies and environmental issues. Phosphate fertilizer production relies almost entirely on the extraction of phosphate rock,[16] a resource that is now facing the risk of depletion. Fast-soluble phosphate fertilizers rapidly provide nutrients to plants, but their high mobility in soil often leads to runoff or leaching into surface water, reducing their availability to plants and causing eutrophication.[17,18] Since 1950, ≈25% of the 250 million tons of phosphate extracted globally has ended up in water bodies or landfills,[19] severely impacting on aquatic ecosystems and threatening biodiversity. This phosphate loss not only reduces fertilizer efficiency but also contributes to environmental pollution.

These issues highlight the inefficiency and environmental risks of current phosphate fertilizer use, emphasizing the urgent need for better phosphorus management. Given the increasing global scarcity of phosphate resources, continued dependence on traditional fertilizers is clearly unsustainable. As a result, slow-release fertilizers, which reduce phosphate loss and improve nutrient use efficiency, have gained increasing attention as a sustainable solution.[20] Slow-release fertilizers use coating technologies to control the release rate, reducing leaching and runoff losses and mitigating environmental impacts.[21] Compared to traditional fast-soluble phosphate fertilizers, slow-release fertilizers can provide a steady supply of phosphate according to plant needs over a longer period, reducing the risk of water eutrophication and improving crop yields. However, existing slow-release fertilizers still rely on phosphate rock as the primary phosphate source, and the issues of phosphate resource depletion and environmental pollution have not yet been addressed.

This study aims to solve the critical issues of phosphorus pollution and resource scarcity by developing a dual-functional adsorbent, the alginate-biochar-calcium hydrogel (ABC-hydrogel), which adsorbs phosphate and reuses it to promote plant growth, thereby alleviating eutrophication at its source and achieving sustainable phosphorus management. Sludge-derived biochar, calcium chloride, and sodium alginate were selected based on their complementary functionalities and their potential to overcome the limitations of individual materials in efficient phosphate removal and slow-release fertilization. Biochar, derived from sewage sludge, is rich in functional groups that have an affinity for phosphate ions. However, biochar is used in fine powder form and poses potential risks due to heavy metal contamination, which hinders its practical application in environmental and agricultural systems.

To address these issues, calcium was introduced to modify the biochar and crosslink alginate, forming a stable hydrogel. The calcium ions not only facilitate phosphate adsorption through ion exchange and precipitation but also stabilize heavy metals within the biochar matrix, reducing their leachability and mitigating environmental risks. During pyrolysis, $CaCl_2$ can promote the formation of volatile metal chlorides (e.g., $ZnCl_2$, $CuCl_2$), which reduces residual metal content.[22] Moreover, calcium can facilitate the transformation of heavy metals into more stable mineral forms, such as Ca-M-OH or Ca-P-M complexes, thereby decreasing their mobility and leachability in the environment.[22,23]This dual function of calcium is crucial for enhancing both the efficiency and safety of biochar in practical applications. Alginate, a natural and biodegradable polymer, was chosen for its ability to form stable hydrogels via calcium crosslinking. In addition to enhancing the mechanical stability of the composite material, alginate significantly improves the water retention capacity of the composite, which is critical for agricultural applications that require sustained moisture release. The swelling capacity of alginate further allows the composite to retain water, supporting plants over extended periods.

Furthermore, the optimal ratio of these materials has been carefully determined using response surface methodology (RSM) to maximize the material's performance in terms of phosphate adsorption. The use of RSM ensures that the combination of these materials is not only effective but also optimized for practical applications, making the use of this composite material a novel and highly efficient solution for sustainable phosphorus management in both water treatment and agriculture.

The specific objectives of this work are to: 1) design and develop an ABC-hydrogel composite material by integrating biochar derived from biological sewage sludge with calcium chloride and sodium alginate; 2) explore the dual function of this material in both efficient phosphorus removal and slow-release fertilization for agricultural use; 3) assess the ability of crosslinking with alginate to enable the ABC-hydrogel to contribute to the safe stabilization of heavy metals in sewage sludge; 4) investigate the slow-release ability and water absorbency of the ABC-hydrogel; and 5) explore the fertilization performance of ABC-hydrogel on lettuce growth. The outcome of this research is intended to provide a novel approach in mitigating phosphorus pollution, facilitating sustainable phosphorus cycling, and promoting sustainable agricultural development while helping to alleviate the depletion of global phosphorus reserves.

To further clarify the novelty of this work, we emphasize that the ABC-hydrogel system goes beyond conventional adsorbent or fertilizer strategies by integrating calcium-modified biochar derived from sewage sludge into an alginate hydrogel matrix. This design enables simultaneous phosphate removal and slow-release fertilization, while addressing heavy metal stabilization and waste reuse. Although biochar-based adsorbents[24,25] and hydrogel nutrient carriers[20,26] have been studied separately, few studies have combined these functionalities into a single, safe, and agriculturally effective material. Our work also includes systematic evaluations from adsorption to plant growth, bridging environmental remediation with agricultural application. These contributions support the ABC-hydrogel's potential as a dual-functional, sustainable solution for circular phosphorus management.

2. Results and Discussion

2.1. Characterization of Biochar and ABC-Hydrogel

Figure S1 (Supporting Information) presents a series of SEM images of sludge and biochar obtained at varying pyrolysis temperatures, magnified 20 000 times. The sludge exhibits a smooth, non-porous surface, primarily due to the presence of organic matter forming a dense, compact structure (Figure S1a, Supporting Information). In contrast, biochar produced at 400–500 °C displays a multilayered structure with dispersed small inorganic particles (Figure S1b,c, Supporting Information). This phenomenon occurs as the surface fatty organic matter decomposes into methane, carbon dioxide, and other gases during pyrolysis, leading to a reduction in surface volume. At this stage, the internal organic components remain largely intact, resulting in a stepped morphology.[27] At 600 °C, a porous structure emerges on the biochar surface, indicating that micropores form as internal volatile gases escape (Figure S1d, Supporting Information). As the pyrolysis temperature increases to 700–800 °C (Figure S1e,f, Supporting Information), the biochar transitions into an aggregate of small particles, primarily due to the extensive decomposition of organic matter at these higher temperatures.[28]

The biochar pyrolyzed at 600 °C is selected to produce ABC-hydrogel as it shows better adsorption capacity than biochar pyrolyzed at other temperatures (Figure S2, Supporting Information). The ABC-hydrogel developed in this study exhibits excellent porosity, with hydrogel beads measuring ≈3.5–4.5 mm in size and pore diameter within the hydrogel being ≈100 µm, as determined by scanning electron microscopy (SEM) (**Figure 1b**). Elemental mapping shows a uniform distribution of Ca, C, and O elements across the cross-section of the hydrogel, indicating that the biochar is uniformly dispersed within the hydrogel (Figure 1c,d,e).

To better understand the elemental transformation during pyrolysis, the major element contents in raw sewage sludge and the resulting biochar (600 °C) were analyzed and compared. As shown in Table S1 (Supporting Information), most key elements, including Al, Fe, Ca, Mg, and P, are significantly enriched in the biochar due to mass loss and thermal concentration effects. For instance, the total phosphorus increased from 17.38 g kg^{-1} in sludge to 32.24 g kg^{-1} in biochar, while calcium increased from 26.92 to 50.76 g kg^{-1}. It has been widely reported that phosphorus in sludge-derived biochar produced at ≥ 600 °C primarily exists in stable mineral forms, such as calcium and iron phosphates, which exhibit low water solubility and limited plant availability.[29] Therefore, in this study, the phosphorus used in adsorption and fertilization experiments was externally added rather than sourced from the biochar itself.

2.2. Response Surface Methodology Design for ABC-Hydrogel Synthesis

Response surface methodology (RSM) plays a crucial role in optimizing experimental conditions while minimizing the number of required experimental runs. By systematically analyzing the interactions between variables, RSM enables the identification of optimal conditions for maximizing phosphate adsorption efficiency. In this study, the optimal ranges for biochar, sodium alginate, and calcium chloride concentrations were first established by pretesting as 0.5–2.5, 5–20, and 10–100 g L^{-1}, respectively. Based on these ranges, 15 experimental sets were designed using RSM, with conditions and results presented in **Table 1**.

The experimental data were fitted to a second-order polynomial model, followed by an analysis of variance (ANOVA) to evaluate the statistical significance of each variable and their interactions. The ANOVA results (Table S2, Supporting Information) indicate that the overall model is statistically significant, with an F-value of 25.60 (greater than the critical value of 3.482 at a significance level of 95%, $\alpha = 0.05$), and a p-value of 0.0012, confirming its adequacy in predicting phosphate adsorption capacity. Among all the terms, the quadratic terms X_1^2, X_2^2, and X_3^2, are found to be statistically significant ($p < 0.05$), indicating their substantial influence on the response variable. A simplified quadratic equation (Equation (1)) is developed to describe the relationship between phosphate adsorption capacity and the significant terms (Y: Adsorption capacity of ABC-hydrogel adsorbent (mg g^{-1}), X_1: Biochar dosage (g L^{-1}), X_2: Sodium alginate concentration (g L^{-1}), X_3: $CaCl_2$ concentration (g L^{-1})):

$$Y = -18.40 + 9.18X_1 + 3.08X_2 + 0.90X_3 - 4.36X_1^2 - 0.13X_2^2 - 0.01X_3^2 \quad (1)$$

The model reveals the nonlinear effects of biochar, alginate, and calcium chloride concentrations on phosphate adsorption capacity, offering valuable insights for hydrogel composite design and optimization. By reducing reliance on excessive trial-and-error experimentation, the RSM model enables efficient formulation optimization and facilitates further adaptations under diverse environmental conditions. The fitted model was used to generate 3D response surface plots (**Figure 2a–c**), which visually illustrate the effects of individual factors and their interactions on phosphate adsorption capacity. The results reveal that when the proportions of sodium alginate, calcium chloride solution, and biochar are 12.25, 53.62, and 1.33 g L-1, respectively, the ABC-hydrogel achieves the optimal phosphate adsorption capacity. A validation experiment conducted under these conditions yielded an adsorption capacity of 31.12 mg g^{-1}, closely matching the predicted value of 30.58 mg g^{-1}, with a low percentage error of 1.7%, confirming the accuracy and reliability of the RSM model.

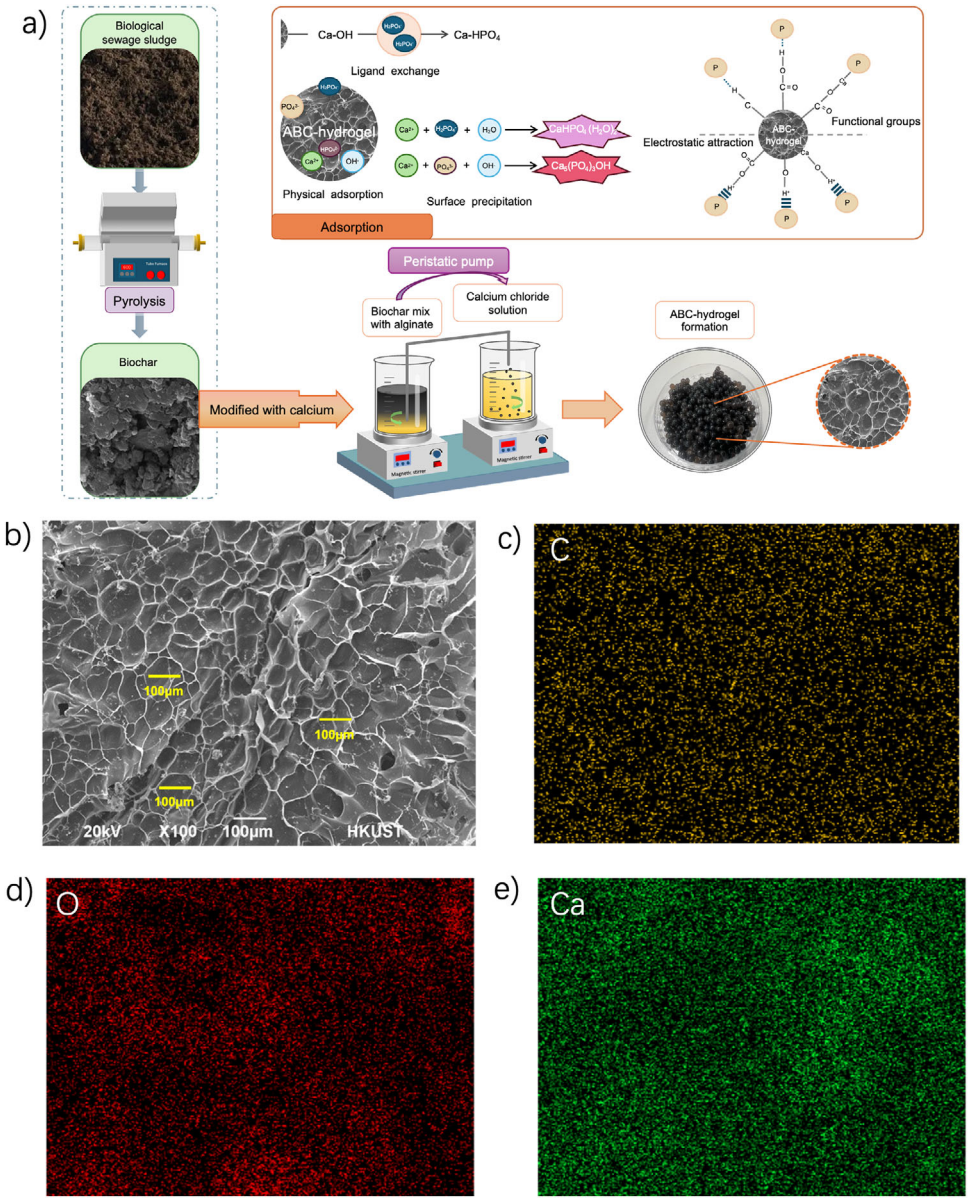

Figure 1. a) Schematic illustration of the preparation of ABC-hydrogel; b) SEM result of ABC-hydrogel; and c,e) EDS distribution of C, O, and Ca elements in ABC-hydrogel.

2.3. Effect of Solution pH, Co-Existing Anions, and Organic Matter on Phosphate Adsorption

One of the advantages of the adsorbent developed in this study is its effective performance across a wide pH range. As illustrated in Figure 2d, the adsorption capacity of the adsorbent for phosphate is ≈42 mg g^{-1} at pH 4–5. When the pH increases to 6–7, the phosphate adsorption capacity decreases to ≈31 mg g^{-1}. However, when the solution pH continues to rise to 8–9, the adsorption capacity of the adsorbent for phosphate rises rapidly to about 60 mg g^{-1}. The speciation of phosphate in solution is pH-dependent: at pH < 2.12, phosphate predominantly exists as H_3PO_4; within 2.12 < pH < 7.21, it primarily exists as $H_2PO_4^-$; in the range 7.21 < pH < 12.31, it is mainly HPO_4^{2-}; and at pH > 12.31, it exists as PO_4^{3-}.[30] The zero charge point (ZCP) of the developed alginate calcium biochar adsorbent was measured to be 6.7 (Figure S3, Supporting Information). When the pH < 6, the adsorbent surface is positively charged, allowing $H_2PO_4^-$ to interact strongly with surface hydroxyl groups via ligand exchange and electrostatic attraction.[31] When the pH is 6–7, the adsorbent itself is neutral, so the electrostatic adsorption capacity is weakened, resulting in a slight decrease in phosphate adsorption capacity. When pH > 7, the adsorption capacity is found to be increased even through electrostatic repulsion between the adsorbent surface and phosphate ions occurs may occur. This is because OH^- in solution facilitates the formation of $Ca_5(PO_4)_3OH$ (hydroxyapatite) through precipitation with Ca^{2+} and HPO_4^{2-}.[31] Therefore, under alkaline conditions, chemical

Table 1. Experimental design conditions and results obtained from RSM for optimizing the phosphate adsorption capacity of ABC-hydrogel.

Run order	Factor 1 Biochar dosage [g L^{-1}]	Factor 2 Sodium alginate concentration [g L^{-1}]	Factor 3 $CaCl_2$ concentration [g L^{-1}]	Response Adsorption capacity [mg g^{-1}]
1	1.50	5.00	100.00	2.05
2	1.50	20.00	100.00	3.55
3	2.50	12.50	100.00	8.79
4	0.50	5.00	55.00	22.63
5	2.50	20.00	55.00	15.52
6	0.50	20.00	55.00	20.76
7	1.50	5.00	10.00	6.92
8	1.50	12.50	55.00	30.00
9	1.50	20.00	10.00	6.43
10	1.50	12.50	55.00	32.73
11	1.50	12.50	55.00	28.62
12	2.50	5.00	55.00	16.27
13	0.50	12.50	100.00	5.45
14	0.50	12.50	10.00	9.83
15	2.50	12.50	10.00	6.59

precipitation is the dominant phosphate adsorption mechanism in the ABC-hydrogel.[32,33]

Considering the presence of common coexisting anions such as Cl^-, NO_3^-, SO_4^{2-}, F^- and CO_3^{2-} in phosphate-contaminated waters, it is crucial to assess the potential effects of these competing ions on the adsorption processes.[34] The results in Figure 2e indicate that increases in the concentrations of NO_3^- and Cl^- exert minimal influence on the phosphorus adsorption capabilities of the adsorbent. Even with ion concentrations reaching up to 10 mmol L^{-1}, the impact on adsorption capacity re-

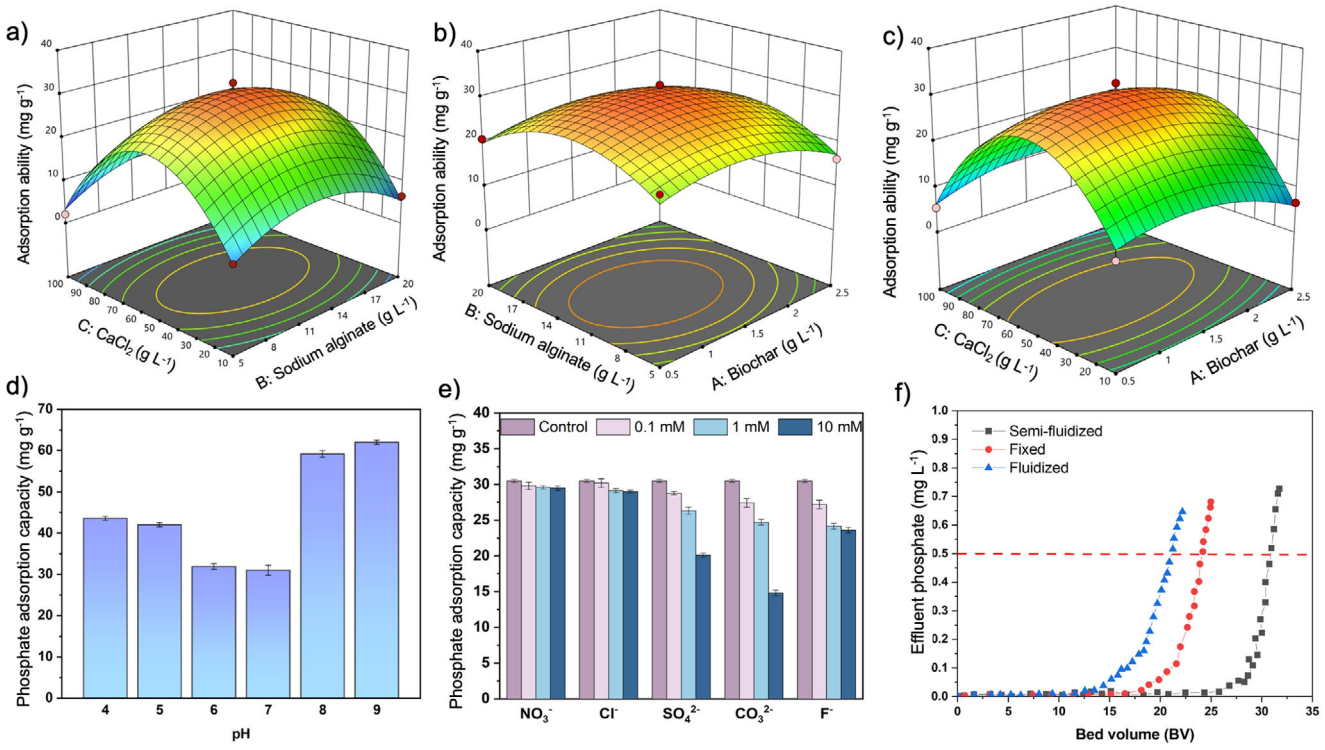

Figure 2. The 3D RSM graphs visually represent the combined influence of a) $CaCl_2$ and sodium alginate, b) sodium alginate and biochar, c) $CaCl_2$ and biochar; d) solution pH, e) coexisting anions effect on phosphate adsorption ability (initial phosphate concentration: 200 mg-P L^{-1}, dosage: 2 g L^{-1}); and f) breakthrough curves of semi-fluidized, fixed, and fluidized columns (pH 7, phosphate concentration of 200 ppm). (Effect of pH and coexisting anions tests were repeated in triplicate, and the data are shown as the mean values with error bars < 5%).

mains marginal, fluctuating between 29.5 and 30.12 mg g^{-1} compared to the control value of 30.5 mg g^{-1}. However, when the F^- concentration increases to 10 mmol L^{-1}, the adsorption capacity decreases to 23.15 mg g^{-1}. The moderate impact of F^- on phosphate adsorption is likely due to their smaller ionic radius and higher charge density, which allows them to compete with phosphate ions and occupy adsorption sites on adsorbent.[35,36] In contrast, CO_3^{2-} demonstrates a notable reduction in phosphate adsorption. As the concentration of CO_3^{2-} increases, the adsorption capacity decreases to 15.13 mg g^{-1}. This is attributed to the high concentration of CO_3^{2-} in the solution, which competes with phosphate ions for adsorption sites to form stable complexes with Ca^{2+} on the adsorbent, reducing the number of effective adsorption sites for phosphate and thereby reducing the phosphate adsorption capacity of ABC-hydrogel. Similarly, SO_4^{2-} also inhibits phosphate adsorption due to its competitive interaction with phosphate ions for the available adsorption sites.[32]

In addition to inorganic ions, natural organic matter may also interfere with phosphate adsorption in real wastewater systems. To further simulate practical conditions, humic acid was introduced as a representative natural organic substance to examine its competitive effect on phosphate adsorption. As shown in Figure S4 (Supporting Information), adsorption capacity decreased with increasing humic acid concentration, from 31.12 to 21.00 mg g^{-1}, dropping by ≈32.5%. This decline is attributed to competitive adsorption between humic acid and phosphate for active binding sites on the adsorbent surface, as well as potential site blockage and complexation effects.[37,38]

2.4. Adsorption Kinetics and Isotherm Study

To assess the adsorption performance of the adsorbent at different temperatures, kinetic and thermodynamic analyses were performed at various temperature conditions (Figure S5a,c, Supporting Information). The pseudo-second-order kinetic model demonstrates a strong fit with the experimental data at all temperatures (Figure S5a, Supporting Information). The equilibrium adsorption capacity (qe) increases with temperature, from 32.82 mg g^{-1} at 20 °C to 48.81 mg g^{-1} at 35 °C, indicating enhanced adsorption at higher temperatures (Table S3, Supporting Information). The rate constant (k) for the pseudo-second-order reaction also increases with temperature, from 1.29×10^{-4} g mg^{-1} min^{-1} at 20 °C to 6.7×10^{-4} g mg^{-1} min^{-1} at 35 °C. This trend shows that the rate of phosphate ion adsorption increases with temperature due to accelerated mass transfer and increased diffusion coefficients at higher temperatures.

The fitted maximum adsorption capacity (q_m) from the Langmuir isotherm model (Table S4, Supporting Information) varied between 190.19 and 252.15 mg g^{-1} across the temperature range of 20–35 °C, indicating that the ABC-hydrogel maintains effective phosphate removal over a broad range of environmental temperatures. Furthermore, the Langmuir equilibrium constant (k_L) increases from 2.94×10^{-4} at 20 °C to 9.48×10^{-4} at 35 °C, further supporting the endothermic nature of the adsorption process.

The thermodynamic parameters, including entropy (ΔS), enthalpy (ΔH), and Gibbs free energy (ΔG) (Equation S1, Supporting Information), are derived using the Van't Hoff equation (Equations S2 and S3, Supporting Information). The enthalpy change (ΔH) is found to be 55.59 kJ mol^{-1}, indicating that the adsorption process is endothermic. The positive entropy change (ΔS = 250.47 J mol^{-1} K^{-1}) indicates increased disorder at the solid-liquid interface during adsorption. Additionally, the negative Gibbs free energy (ΔG) values at all temperatures indicate that the adsorption process is spontaneous.

The ln(k) versus 1/T plot (Figure S5b, Supporting Information) and the ln(K_d) versus 1/T plot (Figure S5d, Supporting Information) provide further insights into the thermodynamic and kinetic aspects of the adsorption. The activation energy (E_a) calculated using the Arrhenius equation (Equation S4, Supporting Information) is determined to be 72.24 kJ mol^{-1}, suggesting that the adsorption process is primarily governed by chemical adsorption, as values exceeding 40 kJ mol^{-1} are generally indicative of chemisorption.

2.5. Adsorption Study in Continuous Flow Systems

The breakthrough curves for the adsorption of phosphate in semi-fluidized, fixed, and fluidized columns are presented in Figure 2f. The breakthrough point is set at a phosphate concentration of 0.5 mg L^{-1}. The data show distinct differences in the performance of each column configuration in terms of the volume of solution processed before reaching the breakthrough point. The semi-fluidized column achieves the highest adsorption efficiency, processing ≈30 bed volumes before reaching the breakthrough phosphate concentration. In comparison, the fixed column reaches the breakthrough point at 24 BV, indicating lower efficiency. The fluidized column demonstrates the lowest adsorption efficiency, with the breakthrough occurring at 18 BV.

The semi-fluidized state optimizes the interaction between the adsorbent particles and the phosphate solution, preventing channeling and agglomeration that are common in fixed columns, thus enhancing the adsorption efficiency.[39–41] By increasing adsorption efficiency by ≈25% compared to the fixed column and 67% compared to the fluidized column, the semi-fluidized column proves to be the most effective configuration for phosphate removal under the test conditions.

In contrast, the fixed column suffers from channeling due to its structure, resulting in an earlier breakthrough and less efficient use of the adsorbent surface area.[42,43] The fluidized column, requiring higher airflow to maintain its state, experiences rapid mixing, reducing the contact time and ultimately leading to the lowest efficiency.[44]

2.6. Phosphate Adsorption Mechanisms

XPS analysis offers valuable insights into the underlying interaction mechanisms between the functional sites of the adsorbent and phosphate. Before adsorption, the binding energies of P $2p_{3/2}$ and P $2p_{1/2}$ are observed at 133.14 and 134.02 eV, respectively (**Figure 3a**). These peaks correspond to different forms of phosphate ions, including free phosphate (PO_4^{3-}) and hydrogen phosphate (HPO_4^{2-}).[45,34] After adsorption, the binding energies of P $2p_{3/2}$ and P $2p_{1/2}$ shift to 132.93 and 133.80 eV, with a significant increase in peak areas, indicating successful phosphate adsorption.[46]

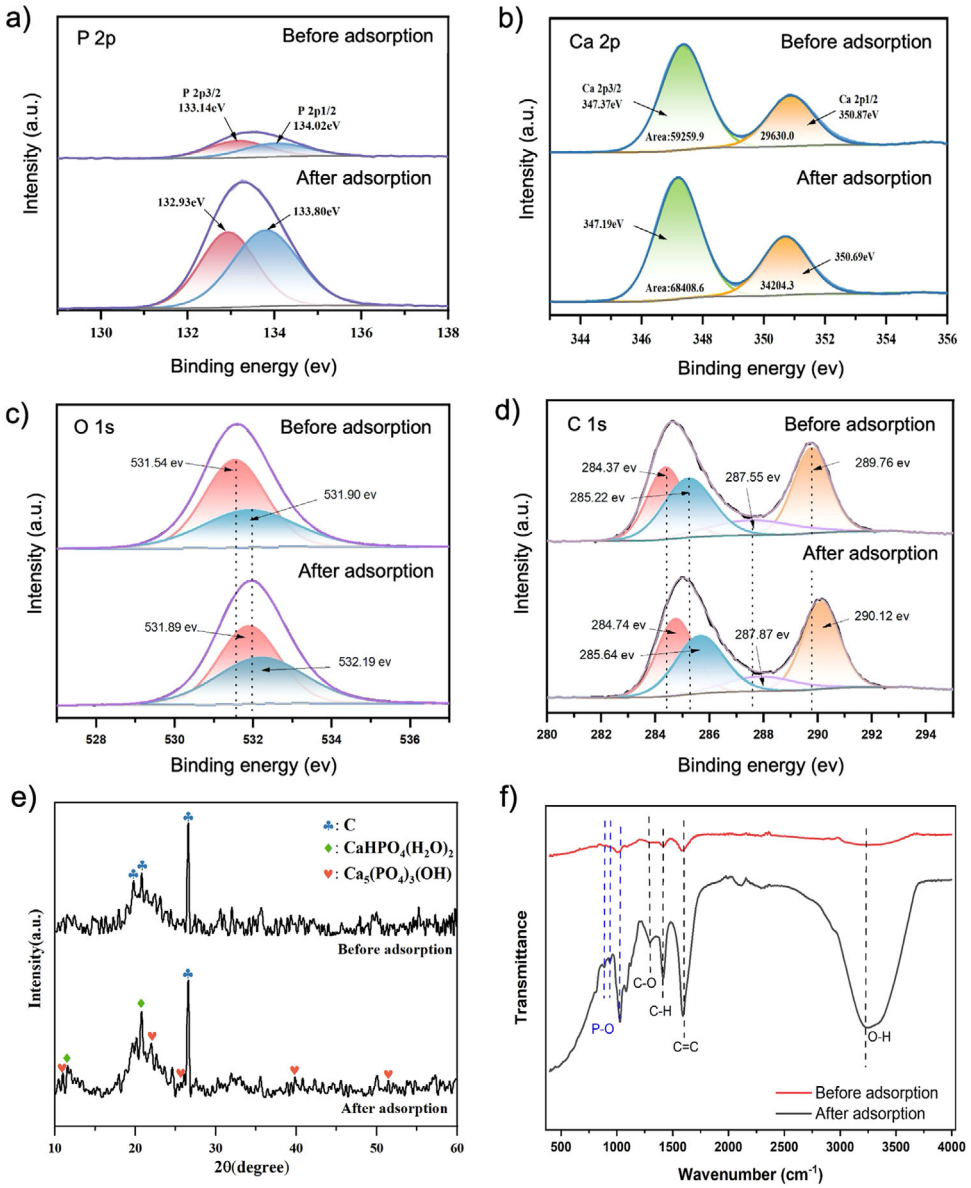

Figure 3. XPS spectra results of a) P 2p, b) Ca 2p, c) O 1s, d) C 1s before and after adsorption; e) XRD results; and f) FTIR results of ABC-hydrogel adsorbent before and after adsorption.

The XPS analysis of calcium (Ca 2p) shows two distinct peaks, Ca $2p_{3/2}$ and Ca $2p_{1/2}$. Before adsorption, the Ca $2p_{3/2}$ peak appears at 347.37 eV, and the Ca $2p_{1/2}$ peak appears at 350.87 eV (Figure 3b). These peaks indicate that calcium is primarily in the form of calcium oxide (CaO) or free calcium ions (Ca^{2+}) before adsorption, associated with surface oxides or carbonates in the biochar.[47] After adsorption, the Ca $2p_{3/2}$ and Ca $2p_{1/2}$ peaks shift slightly, accompanied by larger peak areas. These changes in binding energy and the increase in peak areas indicate that calcium has undergone a chemical transformation due to interaction with phosphate ions during the adsorption process, supporting the formation of a more stable calcium-phosphate compound.[48]

From the XPS O 1s spectra (Figure 3c), the binding energies and peak areas of oxygen change before and after phosphate adsorption on the ABC-hydrogel. Before adsorption, two distinct peaks are observed: one at 531.5 eV, corresponding to hydroxyl (—OH) or carboxyl (-COOH) groups, and another at 531.8 eV, representing oxygen in more structured environments, such as carboxyl groups interacting with calcium.[49] After adsorption, the peaks shift slightly to 531.89 and 532.19 eV. The appearance of the higher energy peak at 532.19 eV, along with an increased peak area, indicates successful phosphate adsorption, with hydroxyl and carboxyl groups involved in the adsorption process.

The C 1s XPS spectra (Figure 3d) reveal significant changes in the binding energies and peak areas of carbon before and af-

ter phosphate adsorption. Before adsorption, peaks at 284.37 and 285.22 eV correspond to C—C/C-H and C—OH/C—O—C groups, while peaks at 287.55 and 289.76 eV correspond to C═O and O═C—O groups from carboxyl and ester functionalities.[50] After adsorption, the peak area at 284.74 eV increases slightly, while peaks at 285.64 and 287.87 eV shift with reduced areas, indicating interactions with phosphate ions. The peak area at 290.12 eV also increases, suggesting that carboxyl groups play an active role in phosphate binding. These changes in binding energy and peak area indicate that the functional groups on the ABC-hydrogel, particularly C—OH, C═O, and O═C—O, are actively involved in the phosphate adsorption process. The reduction in the C═OH and C═O peak areas, along with the shift in binding energy, implies that these groups contributed to phosphate binding through hydrogen bonding and coordination with calcium ions.[34] The increase in the O═C—O peak area indicates that carboxyl groups from the ABC-hydrogel interacted strongly with phosphate, likely forming stable phosphate-calcium complexes and enhancing the overall adsorption capacity of the material.[12]

The XRD results indicate significant structural and compositional changes in the ABC-hydrogel after phosphate adsorption (Figure 3e). After adsorption, new peaks emerged for $CaHPO_4(H_2O)_2$ (brushite) and $Ca_5(PO_4)_3OH$ (hydroxyapatite), confirming the formation of calcium phosphate compounds.[34] The co-existence of brushite and hydroxyapatite reflects a progressive reaction between phosphate ions and calcium, resulting in the precipitation of calcium phosphate species with varying stability. The results reveal the potential of the ABC-hydrogel for effective phosphate adsorption and its transformation into calcium phosphate compounds, which have significant implications for nutrient recovery and recycling. The formation of both brushite and hydroxyapatite demonstrates a two-stage process: brushite, being the less stable and more soluble phase, likely forms initially under slightly acidic or neutral conditions, while hydroxyapatite, which is thermodynamically more stable and has lower solubility, forms over time under near-neutral to alkaline conditions.

For agricultural applications, the release behavior of these compounds as fertilizers is particularly interesting. Brushite is more water-soluble than hydroxyapatite, indicating that it can provide a quicker release of phosphate ions, making it suitable for short-term nutrient supply. On the other hand, hydroxyapatite serves as a slow-release phosphate source, offering long-term nutrient availability while reducing nutrient runoff. The combination of these two phases within the ABC-hydrogel indicates a dual-release system, where brushite addresses immediate nutrient requirements and hydroxyapatite ensures sustained nutrient delivery. These results are consistent with the phosphate slow-release dynamic curve of ABC-hydrogel discussed in Section 2.8.

The FTIR spectra of the ABC-hydrogel, before and after phosphate adsorption, reveal significant changes in the peak intensities and positions, confirming the successful adsorption of phosphate onto the adsorbent surface (Figure 3f). Notable increases in peak intensities are observed at 3226, 1597, 1411, 1288, 1022, 937, and 881 cm^{-1} after adsorption. The peak at 3226 cm^{-1} corresponds to O-H stretching vibrations, indicating enhanced hydrogen bonding or the presence of hydroxyl groups interacting with phosphate ions.[49] The enhanced peak at 1597 cm^{-1} is attributed to asymmetric stretching vibrations of C═C bonds, suggesting that the organic functional groups of the adsorbent provide hydrogen bonding and adsorption sites for capturing phosphate ions.[51] The peaks at 1411 and 1288 cm^{-1} are due to symmetric C-H stretching and C-O stretching vibrations of alcohols or carboxylic acids, further supporting the interaction with phosphate ions. The increase at 1022 cm^{-1}, along with the new peaks at 937 and 881 cm^{-1}, indicates the formation of Ca-O-P stretching vibrations after Ca^{2+} binding to phosphate groups.[34] These changes in the FTIR spectra provide strong evidence of phosphate adsorption onto the ABC-hydrogel, involving hydrogen bonding, surface precipitation, and coordination bonding. The results demonstrate that functional groups on the ABC-hydrogel, including hydroxyl and carboxyl, play a crucial role in phosphate adsorption. The interactions between these functional groups and phosphate ions significantly enhance the hydrogel's ability to adsorb phosphate.

2.7. Heavy Metal Risk Assessment

Figure 4a shows the speciation of heavy metals in raw sludge, biochar, calcium-modified biochar, and ABC-hydrogel and evaluates their ecological risk factors (Figure 4b), pollution factors (Figure 4c), and ecological risk index (Figure 4d). The speciation of heavy metals is a key factor in determining their toxicity and environmental behavior.[52] According to the BCR method, the metal speciation is classified into four categories based on the strength of metal ion binding: exchangeable (F1), reducible (F2), oxidizable (F3), and residual (F4).[53] F1 and F2 represent weakly bound forms of metals, which are unstable and more readily bioavailable, while F3 and F4 are strongly bound forms that are more stable and less bioavailable.

As shown in Figure 4a, the forms of heavy metals in the raw sludge are mainly unstable forms (F1 and F2). Among these, Mn has the highest concentration at 93.31%, while Cu has the lowest at 9.43%. Other metals show the following activity levels: Cr (32.73%), Ni (86.15%), and Zn (75.97%). This suggests that the direct utilization of sewage sludge presents a potential risk of heavy metal pollution. However, after pyrolysis at 600 °C for 1 h to form biochar, the F1 and F2 species gradually transform into more stable F3 and F4 forms. This indicates that high temperatures facilitate the transformation of heavy metals into more stable binding states.[27] Calcium modification and hydrogel crosslinking treatments further reduce the proportion of F1 and F2 in the material, converting these metals into more stable F3 and F4 forms. This is because calcium chloride modification additives can form low-boiling volatile compounds (such as $ZnCl_2$) with heavy metals (such as Zn, Cu, etc.), thereby promoting the volatilization of these metals at high temperatures and reducing their concentrations in biochar residual.[22] Additionally, sodium alginate hydrogel itself also exhibits adsorption ability for heavy metals, and its network structure further reduces metal mobility.[54]

Based on the BCR results, the risk factor (Er), pollution factor (Cf), and ecological risk index (RI) of heavy metals were calculated to further evaluate the environmental safety of the adsorbent and ensure its valuable role in converting sludge into a safe and sustainable resource. The results show that the calcium-modified biochar and hydrogel crosslinking treatments are sig-

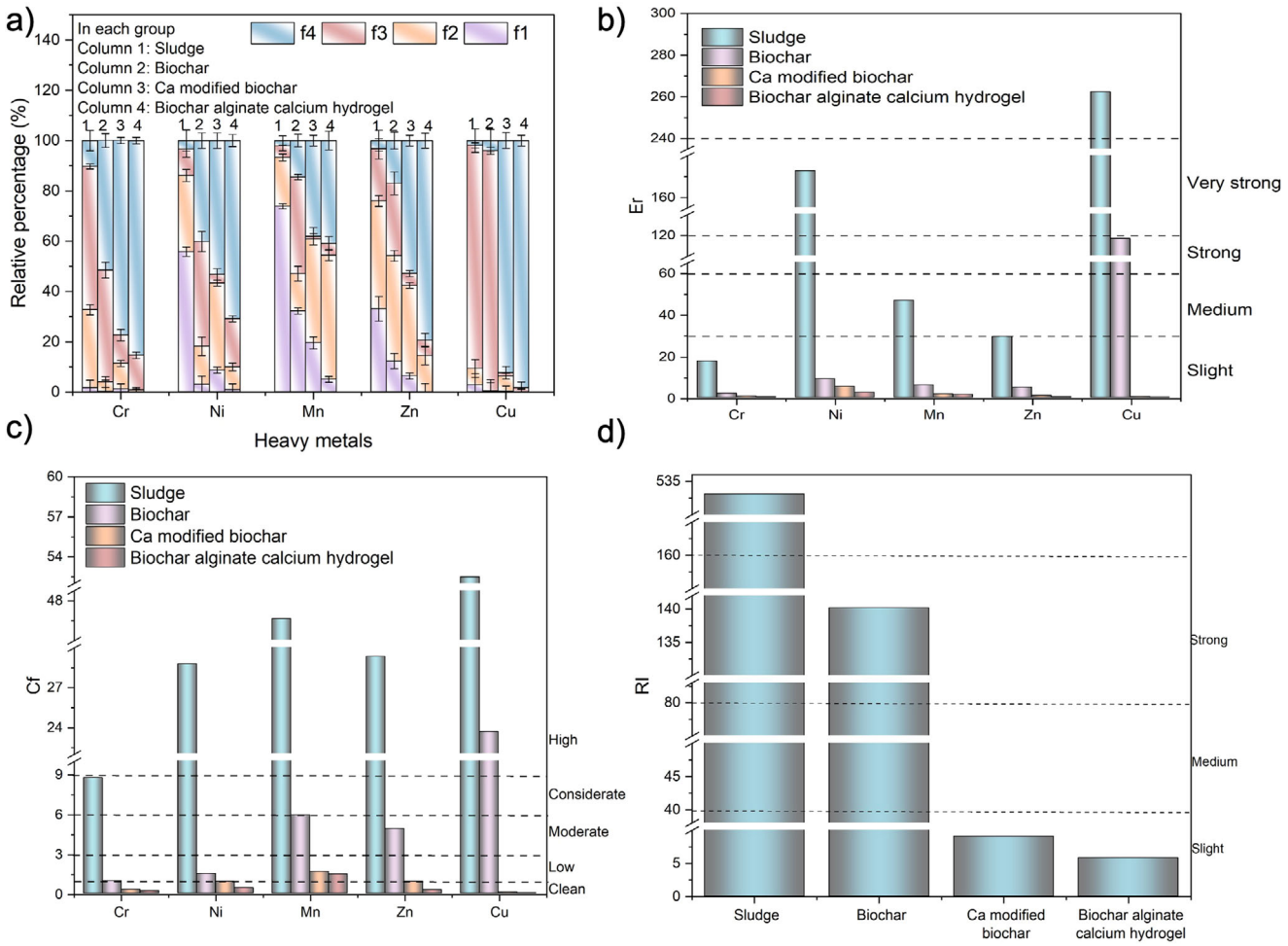

Figure 4. a) The BCR sequential extraction (F1: Exchangeable, F2: Reducible, F3: Oxidizable, F4: Residual); b) Heavy metal ecological risk factor; c) Heavy metal pollution factor; and d) Overall ecological risk index of sludge, biochar, calcium-modified biochar, ABC-hydrogel. (The BCR sequential extraction experiments were conducted in triplicate, and the data are shown as the mean values with error bars < 5%).

nificantly more effective than the unmodified biochar in reducing all risk factors, lowering their levels from "strong" to "slight" or even "clean".

Figure 4d shows that the ecological risk index (ERI) decreases significantly as the material transitions from untreated sludge to biochar, calcium-modified biochar, and ABC-hydrogel. The ERI dropped dramatically from 533.13 in the raw sludge to 140.20 in biochar, 9.02 in calcium-modified biochar, and 5.79 in ABC-hydrogel, indicating a substantial reduction in ecological risks associated with heavy metals through pyrolysis, calcium modification, and alginate crosslinking. The ecological risk level decreased from "strong" to "slight," highlighting the enhanced effectiveness of ABC-hydrogel in mitigating ecological risks associated with heavy metals.

These results highlight the fact that the ABC-hydrogel adsorbent developed in this study not only significantly reduces the ecological risks of heavy metals but also offers enhanced stability and safety. Compared to other treatment forms, it achieves lower ERI values, underscoring its exceptional effectiveness in heavy metal stabilization. In addition to its environmental benefits, the ABC-hydrogel also complies with the Chinese national control standards of pollutants in sludge for agricultural use (GB 4284-2018, Level A) (**Table 2**). This makes the ABC-hydrogel a safe and effective fertilizer for sustainable agriculture. It not only converts sewage sludge into a safe and valuable resource, serving as an efficient phosphate removal adsorbent but also functions as a fertilizer, benefiting crops such as vegetables, grains, oil crops, fruit trees, fodder crops, and fiber crops.

2.8. Slow-Release Ability of ABC-Hydrogel as a Fertilizer

The phosphate release behavior of the ABC-hydrogel is illustrated by the schematic in **Figure 5a**, and the corresponding dynamic release curve is shown in Figure 5b. The results demonstrate the hydrogel's excellent slow-release capability, with ≈48% of the phosphate being released over a 37-day period. In comparison, biochar released only ≈12% of its phosphate content in the same time frame, indicating a significantly slower release rate. These results highlight the enhanced phosphate retention and gradual release provided by the ABC-hydrogel, making it an ideal candi-

Table 2. The heavy metal contents of biological sludge and ABC-hydrogel, together with the Chinese national standard GB 4284–2018.

	Zn mg kg^{-1}	Cu mg kg^{-1}	Ni mg kg^{-1}	Cr mg kg^{-1}	Mn mg kg^{-1}	Pb mg kg^{-1}	Cd mg kg^{-1}	Hg mg kg^{-1}	As mg kg^{-1}	Ref.
Biological sludge	385	166	90.5	73.2	831	–	–	–	–	This study
ABC-hydrogel	103.27	73.18	58.07	48.99	294.05	–	–	–	–	This study
Chinese national standard (GB 4284–2018[a], level A[b])	<1200.00	<500	<100	<500	Not mentioned	<300	<3	<3	<30	GB 4284–2018

[a] GB 4284-2018: Control standards of pollutants in sludge for agricultural use; [b] Level A sludge products: The types of agricultural land permitted include arable land, garden land, and pastureland. Allowed for use on vegetables, grain crops, oil crops, fruit trees, fodder crops, and fiber crops.[55]

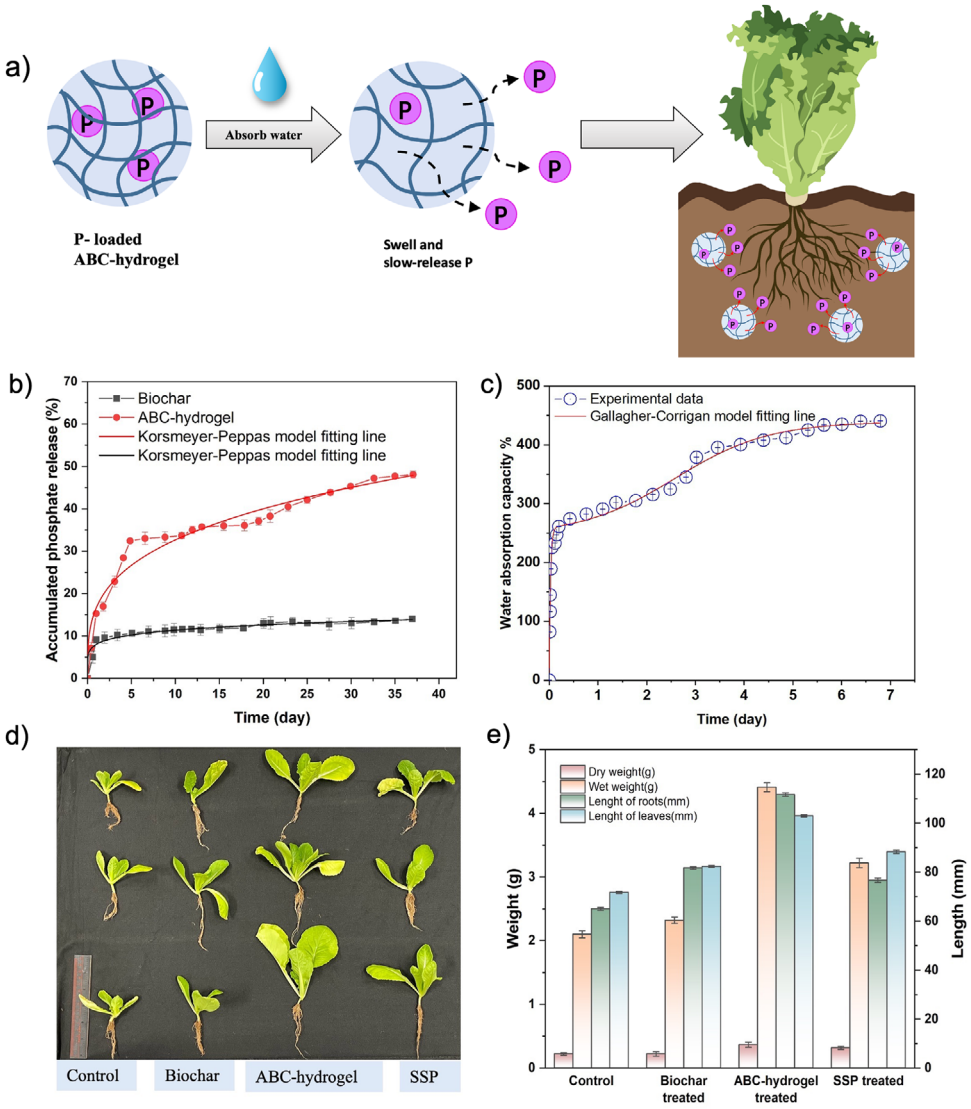

Figure 5. a) Schematic diagram illustrating the functions of the ABC-hydrogel as fertilizer; b) the slow-release dynamic curve of biochar and ABC-hydrogel; c) water swelling dynamic curve of ABC-hydrogel; d) photo of lettuce samples, and e) comparison of wet weight, length of roots and leaves of lettuce in control, biochar treated, ABC-hydrogel treated and SSP treated groups. (All the tests were repeated in triplicate, and the data are shown as the mean values with error bars < 5%).

Table 3. Kinetic fitting parameters of phosphate slow-release for ABC-hydrogel and biochar.

Material	k [rate constant]	n [exponent]	R^2	Transport mechanisms
Biochar	8.01	0.15	0.96	Fickian diffusion
ABC-hydrogel	16.66	0.29	0.96	Fickian diffusion

date for applications where controlled nutrient release is essential.

To further describe the release behavior, the dynamic release curve of both ABC-hydrogel and biochar is fitted using the Korsmeyer-Peppas model, which is commonly used to model drug release and slow-release materials. The fitting is good, with a high R^2 value of 0.96, indicating a strong correlation to the model. The fitting parameters for ABC-hydrogel are found to be $k = 16.66$ and $n = 0.29$. The value of n suggests that the phosphate release mechanism follows a Fickian diffusion process, which is characteristic of molecular diffusion-controlled release. This shows that the release of phosphate from the ABC-hydrogel is primarily governed by the diffusion of phosphate ions through the hydrogel matrix over time.

In contrast, biochar exhibits a slower release profile, with a rate constant of $k = 8.01$ and a higher exponent $n = 0.15$ (**Table 3**). This also indicates a Fickian diffusion mechanism but with a much slower release rate compared to the ABC-hydrogel. The lower values of k and n suggest that while biochar is capable of slowly releasing phosphate, the process is less efficient, leading to a longer duration for phosphate to be made available to plants.

While both the ABC-hydrogel and biochar exhibit slow-release properties, the different release rates can make them more suitable for different plant growth requirements. For instance, the higher release rate of phosphate from the ABC-hydrogel can be more suited for plants with a higher short-term nutrient demand, providing them with a sufficient supply of phosphate for quicker growth. On the other hand, biochar's slower release profile, although beneficial for sustained long-term nutrient supply, cannot meet the immediate phosphate needs of fast-growing crops. This observation aligns with the results of the lettuce growth experiments discussed in Section 2.10, where biochar is found to be inadequate for supporting optimal growth in plants with a short growth cycle, such as lettuce.

2.9. Water Absorbency Study of ABC-Hydrogel

The results demonstrate that the ABC-hydrogel exhibits exceptional water absorption capacity, achieving a maximum absorption of 439.22% within ≈6 days (Figure 5c). This performance is characterized by an initial rapid swelling phase, followed by a slower, more steady absorption process. To quantify this biphasic behavior, the Gallagher–Corrigan model was employed. This model is particularly suitable for describing the complex absorption kinetics of hydrogels as it accounts for both the fast initial uptake and the slower, sustained absorption phase. The model fit is excellent, with an R^2 value of 0.99, providing reliable quantitative insights into the hydrogel's absorption kinetics.

The fitted parameters further emphasize the material's strong initial water uptake, which is crucial for improving soil moisture retention and supporting long-term plant growth. The initial absorption capacity $(f_1)_B$ of 246.83% and the maximum absorption $(f_1)_{max}$ of 439.22% suggest that the hydrogel rapidly absorbs water initially and reaches its saturation point. Additionally, the stage I rate constant (Kg,1) of 35.21 indicates a fast initial uptake, while the stage II rate constant (Kg,2) of 1.03 reveals a significantly slower, sustained absorption phase (**Table 4**).

Table 4. Kinetic fitting parameters of the Gallagher–Corrigan model of ABC-hydrogel.

Parameters	Values
$(f_1)_B$	246.83
Kg,1	35.21
Kg,2	1.03
$(f_1)_{max}$	439.22

This dual-phase absorption behavior is particularly advantageous for applications in agriculture. Such characteristics make it highly suitable for use as a slow-release fertilizer, particularly in arid and water-scarce regions or in soils with poor water retention capacity. These findings underscore the excellent potential of the ABC-hydrogel as a sustainable and efficient solution for water management in agriculture, contributing to improved soil moisture retention and enhancing plant growth in challenging environmental conditions.

2.10. Lettuce Seed Germination and Growth

To investigate the impact of the ABC-hydrogel on plant growth, lettuce was selected for its rapid growth cycle and global popularity as one of the most widely grown vegetables. Both seed germination and plant cultivation tests were conducted to assess the hydrogel's effectiveness in promoting early seedling development and overall growth.

The seed germination results demonstrate a notable increase in germination rates with the addition of P-loaded ABC-hydrogel. In the baseline control, seeds in deionized water exhibit a germination rate of 74%. The addition of P-loaded calcium-modified biochar enhanced the germination rate to 84%. Most notably, the P-loaded ABC-hydrogel treatment achieved the highest germination rate of 88%, suggesting that the ABC-hydrogel improves seed germination and contributes positively to early seedling growth. This enhancement is particularly significant as it demonstrates the hydrogel's ability to accelerate the early stages of plant development.

For the pot cultivation experiment shown in Figure 5d, four treatment groups were established: the control group, the P-loaded calcium-modified biochar treated group, the P-loaded ABC-hydrogel treated group, and the SSP treated group. SSP (single superphosphate) is a commonly used commercial phosphorus fertilizer that serves as a benchmark to compare the effectiveness of our sustainable adsorbent materials. As shown in Figure 5e, the control group, which lacks any added phosphorus source, exhibits the poorest growth conditions. In contrast, the addition of phosphorus through calcium-modified biochar and P-loaded ABC-hydrogel significantly improves the plant growth

parameters, including leaf length, root length, wet weight, and dry weight.

Among all the treatments, the P-loaded ABC-hydrogel group shows the most pronounced improvements. Specifically, this group achieves the highest wet weight (4.41 g), dry weight (0.37 g) the longest root length (111.70 mm), and the largest leaf length (103.10 mm). The P-loaded ABC-hydrogel treatment led to a substantial increase in growth metrics compared to the control group, including an increase in wet weight by 110%, dry weight by 65%, length of root by 72%, and length of leaves by 44%. These results underscore the hydrogel's significant role in promoting plant growth, attributed to its ability to moisturize and continuously provide nutrients, as discussed in Sections 2.8 and 2.9.

In comparison, the biochar-treated and SSP-treated groups show moderate improvements. The biochar treatment results in a root length of 81.70 mm and a wet weight of 2.32 g, while the SSP treatment shows better performance in leaf length (88.30 mm) but is less effective overall compared to the hydrogel treatment. The control groups consistently exhibit the lowest values across all growth parameters, with a wet weight of 2.10 g, dry weight of 0.20 g, a root length of 65.02 mm, and a leaf length of 71.70 mm, indicating suboptimal growth conditions without any nutritional additions.

The findings highlight the superior effectiveness of ABC-hydrogel composites in enhancing plant biomass and development. The hydrogel's ability to retain water and improve nutrient availability makes it a highly promising soil amendment for improving plant growth outcomes. The results from both seed germination and cultivation tests emphasize the potential of ABC-hydrogel as a sustainable solution in agricultural practices, enhancing both seedling establishment and plant growth.

3. Conclusion

This study introduces a dual-functional ABC-hydrogel as an efficient material for both phosphate removal and slow-release fertilization, contributing to the advancement of phosphorus management and sustainable agricultural development. The key findings of this study include the exceptional phosphate adsorption capacity of the ABC-hydrogel, which can reach up to 252.15 mg g^{-1} at 20 °C, and its significant role in enhancing seed germination and lettuce growth. The P-loaded ABC-hydrogel significantly enhances lettuce seed germination, increasing the germination rate from 77% to 88%. Furthermore, compared to the control group, it substantially improves key plant growth parameters, resulting in a 110% increase in wet weight, a 65% increase in dry weight, a 72% increase in root length, and a 44% increase in leaf length. Furthermore, the hydrogel exhibits superior slow-release behavior, with ≈48% of the phosphate being released over a 37-day period, offering a controlled nutrient supply for plant growth.

The environmental impact of the ABC-hydrogel is also thoroughly assessed. The treatment method proposed in this study, including pyrolysis, calcium modification, and crosslinking in hydrogel, effectively reduces the ecological risk of heavy metals in sewage biological sludge. The ecological risk index drops significantly from 533.13 in untreated sludge to 5.79 in the ABC-hydrogel, highlighting its potential for safe and sustainable use in agricultural practices. The ABC-hydrogel also meets the Chinese national standards GB 4284-2018, Level A, ensuring its suitability for use as a fertilizer in agricultural soils.

This work contributes significantly to advancing phosphorus removal technology by presenting a sustainable solution for phosphorus recovery and slow-release fertilization. The use of waste-derived materials such as biochar in the development of the ABC-hydrogel promotes circular economy practices, converting sewage sludge into a valuable resource for agricultural and environmental applications. With a maximum water absorption capacity of 439.22%, the hydrogel can effectively retain water, enhancing soil moisture availability in arid and drought-prone areas. This property makes it a promising solution for improving water retention in agricultural soils, reducing irrigation frequency, and supporting plant growth under water-limited conditions. The hydrogel's dual functionality as both an adsorbent and a slow-release fertilizer opens new possibilities for sustainable agriculture, particularly in regions facing challenges related to soil nutrient depletion, water scarcity, and the need for eco-friendly fertilizers.

It is recommended that future studies focus on further optimizing the ABC-hydrogel to enhance its long-term reusability and reduce costs. The long-term performance of the ABC-hydrogel in soil, including the biodegradation behavior of alginate, its effect on nutrient release, soil chemistry, and the potential for heavy metal leaching, warrants further investigation under realistic field conditions. Future work should also examine whether the ABC-hydrogel can be reused as an adsorbent after its initial phosphate release, enabling multiple cycles of capture and utilization. Additionally, adjusting the material composition, particularly the ratio of biochar to alginate and the crosslinking density, offers a promising strategy to tailor phosphate release profiles to match crop-specific nutrient uptake patterns. This direction is supported by our findings that the ABC-hydrogel exhibits diffusion-controlled release behavior, which is sensitive to the internal structure governed by its formulation. Future work should also evaluate the performance of the ABC-hydrogel in real wastewater systems, where complex water matrices may affect adsorption efficiency and material stability. The development of other waste-derived adsorbent-fertilizer systems can be explored to address the phosphate contaminants in aquatic systems and the shortage of phosphorus in agriculture. Expanding the application of the ABC-hydrogel to diverse agricultural contexts, including large-scale farming, would further demonstrate its effectiveness in improving crop yields while minimizing environmental impact. Overall, the ABC-hydrogel developed in this study represents a significant step toward achieving sustainable agricultural practices and environmental remediation, making it a very promising solution for addressing the global issues of phosphorus pollution and phosphate resource scarcity.

4. Experimental Section

Chemicals and Materials: Details of the chemicals and reagents used in this study are listed in Table S5 (Supporting Information), and they were all used without prior purification. All solutions were prepared using deionized (DI) water unless stated otherwise.

Synthesis and Characterization of Biochar and ABC-Hydrogel—Pyrolysis and Modification of Biochar: The biological sludge samples were collected from a wastewater treatment plant in Hong Kong using clean,

non-contaminating tools. Two sampling events were conducted with a one-month interval between them. The samples from both events were thoroughly mixed to ensure uniformity and then stored in clean, airtight bottles at 4 °C to preserve them until analysis. The sludge was first dried in an oven at 110 °C for 12 h until a constant weight was achieved (ASTM D2216 standard method) to ensure consistent sample weight before being subjected to pyrolysis.

To determine the optimal pyrolysis temperature for biochar, dried sludge was pyrolyzed for 1 h under a nitrogen atmosphere at temperatures of 400, 500, 600, 700, and 800 °C. The produced biochar was ground and sieved through a 100-mesh screen to achieve a fine and uniform particle size for phosphate adsorption. All adsorption batch studies were conducted with a solid-to-liquid ratio of 2 g L^{-1} in 200 ppm phosphate stock solutions. The pH of the solution was adjusted to 7, and the adsorption time was set to 12 h. All batch tests were conducted in triplicate to verify their consistency, and the data obtained had standard deviations below 5%, ensuring precision.

As shown in Figure S2 (Supporting Information), the biochar pyrolyzed at 600 °C exhibits the highest phosphate adsorption capacity and was selected for further modification. To determine the optimal calcium chloride concentration for biochar modification, biochar pyrolyzed at 600 °C was first treated with 1 mol L^{-1} NaOH for 2 h to enhance the surface area and porosity and remove impurities. It was then modified with calcium chloride solutions at concentrations of 1, 2, 3, 4, 5, and 6 mol L^{-1}. The solid-to-liquid ratio was 7 g L^{-1}, and the treatment time was 6 h.

As shown in Figure S6 (Supporting Information), the biochar treated with a 3 mol L^{-1} calcium chloride solution shows the highest phosphate adsorption capacity and was selected for the preparation of the ABC-hydrogel adsorbent in this study.

Experimental Design for ABC-Hydrogel Synthesis Using Response Surface Methodology: In this study, Box–Behnken Design (BBD), a widely used experimental design within response surface methodology (RSM), was employed to optimize the composition of the ABC-hydrogel in terms of its phosphate adsorption capacity. BBD was selected due to its efficiency in evaluating quadratic response surfaces with a reduced number of experimental runs compared to full factorial designs. Moreover, it avoids experimental combinations where all factors are simultaneously at their extreme levels, which was particularly beneficial for ensuring the stability of hydrogel formulations.

The objective of the design was to determine the optimal composition of the three key components – biochar, calcium, and alginate – to maximize the phosphate removal capacity of ABC-hydrogel. Three independent variables were selected based on their critical roles in determining the adsorption performance of the ABC-hydrogel: Biochar dosage (X_1) – contributes to surface area, porosity, and active functional groups for phosphate binding; Calcium concentration (X_2) – contributes to hydrogel matrix formation and affinity to phosphate ions; Alginate content (X_3) – affects the gel structure, mechanical integrity, and diffusivity of phosphate ions within the hydrogel. Each variable was studied at three coded levels (−1, 0, +1), and the experimental design had a total of 15 runs, including three replicates at the center point to estimate experimental error. The total number of experiments (N) required by BBD for three factors is calculated using Equation (2):

$$N = 2k\,(k-1) + C_0 \tag{2}$$

where k is the number of factors (3 in this study), and C_0 is the number of center point replications (3 in this study).

The relationship between the response (Y, phosphate adsorption capacity) and the independent variables (X_1: biochar dosage, X_2: calcium concentration, X_3: alginate content) was modeled using a second-order polynomial regression model. The general form of the model is shown in Equation (3):

$$Y = \beta_0 + \sum_{i=1}^{k} \beta_i X_i + \sum_{i=1}^{k} \beta_{ii} X_i^2 + \sum_{i=1}^{k} \sum_{j=i+1}^{k} \beta_{ij} X_i X_j + \varepsilon \tag{3}$$

where Y is the predicted response (phosphate adsorption capacity), X_i and X_j are the coded levels of the independent variables, β_0 is the intercept term, β_i,β_{ii}, and β_{ij} are the linear, quadratic, and interaction coefficients, respectively, ε is the residual error term.

The response variable (Y) used for optimization was the phosphate adsorption capacity (mg g^{-1}), which was measured in all runs. Design-Expert software was used for data analysis. Data obtained from the experiments were fitted to a second-order polynomial model, and analysis of variance (ANOVA) was used to assess the significance of each variable and their interactions. The fitted model was then used to generate response surface plots to visualize the effect of individual factors and their interactions and to determine the optimal formulation.

Synthesis of ABC-Hydrogel: In accordance with the RSM design, 1.325 g L^{-1} of biochar and 12.250 g L^{-1} of sodium alginate were thoroughly mixed for 4 h to achieve a homogeneous blend. The mixture was then dripped into a 53.620 g L^{-1} calcium chloride solution using a peristaltic pump at a flow rate of 20 mL min^{-1}, followed by stirring for 2 h. The alginate-biochar to calcium chloride ratio was maintained at 1:4. To ensure complete cross-linking, the mixture was stored overnight in a refrigerator at 4 °C. Finally, the hydrogel was freeze-dried for 6 h to obtain the ABC-hydrogel adsorbent, as illustrated in Figure S7 (Supporting Information). The process flow diagram is shown in Figure 1a.

Characterization of Biochar and ABC-Hydrogel: The morphological characteristics of the biochar and ABC-hydrogel adsorbent were examined using a scanning electron microscope (SEM, JEOL JSM-6390), coupled with an Energy Dispersive X-ray Spectrometer (EDS, Bruker Quantax 70). To investigate the functional groups present in the adsorbent, Fourier Transform Infrared Spectroscopy (FT-IR, Bruker Vertex 70, USA) was employed. The chemical composition of the adsorbent was further analyzed by X-ray Photoelectron Spectroscopy (XPS, Thermo Scientific K-Alpha, USA). Additionally, the crystal structure of the adsorbent, both before and after adsorption, was evaluated using X-ray Diffraction (XRD, Philips PW-1830).

Experimental Setup and Phosphate Adsorption Tests—Batch Study: Phosphate adsorption experiments were conducted in 50 mL polypropylene conical tubes. Phosphate solutions were prepared by dissolving potassium phosphate to achieve a concentration of 200 mg-P L^{-1}, which was selected to simulate the phosphate concentration typically found in wastewater from fertilizer facilities.[56,57] For all the adsorption experiments, except those focused on pH effects, the solution pH was maintained at 7.0 ± 0.1 by adjusting with HCl and/or NaOH. Samples were agitated at a constant rotational speed of 50 ± 1 rpm at room temperature, except for experiments specifically designed to investigate temperature effects.

To investigate the effect of pH on phosphate adsorption, 2 g L^{-1} of adsorbents were tested in 200 ppm phosphate solutions across a pH range of 4–9. To assess the influence of coexisting anions on phosphate adsorption, nitrate, chloride, sulfate, carbonate, and fluoride ions were individually added to the phosphate solution at concentrations of 0.1, 1, and 10 mmol L^{-1}.

The impact of temperature on the adsorption process was studied at four temperatures: 20, 25, 30, and 35 °C. The adsorption data were fitted to the Langmuir isotherm model (Equation S5, Supporting Information) to determine the adsorption equilibrium. The thermodynamic feasibility of the adsorption process was further analyzed by calculating the changes in Gibbs free energy (ΔG), entropy (ΔS), and enthalpy (ΔH) using Equations S1–S3 (Supporting Information), respectively. The adsorption kinetics at different temperatures were modeled using the pseudo-second-order kinetic model (Equation S6, Supporting Information).

Before taking measurements, the samples were allowed to settle for 15 min, after which the phosphate concentrations were measured using the molybdenum blue method at 700 nm with a UV–vis spectrophotometer (Hitachi UH5300). All experiments were conducted in triplicate with a standard deviation lower than 5% to ensure the reliability and reproducibility of the results.

Continuous Flow Study: The adsorption experiments were conducted in a fixed bed, fluidized bed, and semi-fluidized bed using columns with a height of 10 cm and a diameter of 2 cm, resulting in a bed volume of

31.42 mL. Each column was loaded with 8 g of adsorbent, and the phosphate concentration in the solution was maintained at 200 ppm. To ensure a semi-fluidized state, the airflow rate was set at 0.5 mL min^{-1}, and the liquid flow rate was maintained at 1.5 mL min^{-1}. For the fixed column and fluidized column experiments, the liquid flow rate was kept constant at 1.5 mL min^{-1}, the same as for the semi-fluidized columns. To maintain a fluidized state in the fluidized column, the airflow rate was adjusted to 3 mL min^{-1}. Effluent solutions were collected every 5–10 min, and the phosphate concentration was measured using the molybdenum blue method. The breakthrough point was set at a phosphate concentration of 0.5 mg L^{-1} to meet the Chinese effluent discharge standard.

Heavy Metal Test Experiments and Ecological Risk Assessment: The total concentrations of heavy metals in the sludge samples were determined by ICP-OES following HNO_3 + $HClO_4$ (70%) + HF acidic digestion. The values were expressed as mg of metal per kg of dry sludge, using Equation S7 (Supporting Information). To assess the mobility, bioavailability, and potential environmental impact of the heavy metals in the adsorbent in this study, a BCR (Bureau Community Reference) sequential extraction test was conducted. The BCR sequential extraction method was a standardized procedure used to fractionate metals in environmental samples into different chemical forms to reflect their potential mobility and bioavailability. The specific extraction steps are listed in Text S1 (Supporting Information). All BCR sequential extraction experiments were conducted in triplicate, and the data are shown as the mean values with error bars < 5%.

Lettuce seed germination and Growth Experiment: To assess the impact of the reused adsorbent on lettuce seed germination, three treatments were tested, each repeated three times. The treatments included a control group (no additives), P-loaded calcium-modified biochar, and P-loaded ABC-hydrogel. Fifty lettuce seeds were placed on moistened filter paper in Petri dishes containing deionized water. The experimental conditions were as follows: no material (control group), 0.01 g of calcium-modified biochar, and 0.01 g of ABC-hydrogel. All treatments were incubated at room temperature. On the third day, the number of germinated seeds was counted.

For the pot cultivation experiment, each pot was filled with 300 g of uniformly mixed coconut soil, and four different treatments were applied: control group (no additives), P-loaded biochar, P-loaded ABC-hydrogel, and SSP, with three replicates for each treatment. The cultivation duration was ≈1 month from seedling emergence to harvest. Each pot received 50 mg of phosphate in total. Based on their respective phosphate loading capacities (biochar = 20.5 mg g^{-1}; ABC-hydrogel = 31.2 mg g^{-1}), 2.44 g of biochar or 1.60 g of ABC-hydrogel was applied per pot to ensure equal phosphorus input across treatments. No additional material was added to the control group. The pots were irrigated weekly with 350 mL of water, and all were kept under identical environmental conditions, including temperature, humidity, and light duration. After the plants were harvested, the average root length, leaf length, wet weight, and dry weight were measured in triplicate using a ruler and a digital balance with a precision of ± 0.0001 g to evaluate the overall growth and biomass production. All lettuce measurements were performed by the same researcher to maintain consistency, and data were shown as the mean values with a standard deviation below 5%.

Slow-Release Rate of Biochar and ABC-Hydrogel: For phosphorus release testing, 0.2 g of phosphate-loaded adsorbent (either biochar or ABC-hydrogel) was immersed in 100 mL of deionized water in sealed containers and kept at ambient temperature (22 ± 1 °C). The solid-to-liquid ratio was 2 g L^{-1}. Phosphate loading levels are 20.5 mg g^{-1} for biochar and 31.2 mg g^{-1} for ABC-hydrogel, determined from prior adsorption experiments. At predetermined intervals, 3 mL of supernatant was withdrawn, filtered, and analyzed using the molybdenum blue method. The cumulative release was calculated as a percentage of total loaded phosphorus. All tests were conducted in triplicate. The dynamic release curves were fitted using the Korsmeyer-Peppas model, which describes the release process from a matrix as a function of time. Model fitting accuracy was evaluated using the coefficient of determination (R^2). The equation for the model is shown below (Equation (4)):

$$f(t) = k \cdot t^n \quad (4)$$

f(t) represents the cumulative release percentage at time t, k represents the rate constant, and n is the release exponent, which helps identify the release mechanisms (Fickian diffusion, Case II, or anomalous transport).

The fitting of this model to the experimental data was carried out for both biochar and ABC-hydrogel. The parameters k and n and the corresponding transport mechanisms were identified. In particular, the value of the exponent n helps classify the mechanisms of release:

$n \leq 0.5$: Fickian diffusion, which is characterized by molecular diffusion.

$0.5 < n < 1$: Anomalous transport, a combination of diffusion and polymer relaxation or swelling.

$n = 1$: Case II transport, typically related to polymer erosion or relaxation.

$n > 1$: Super Case II transport, dominated by relaxation or erosion.

Water Absorbency Test: The water absorbency of the ABC-hydrogel was assessed through a gravimetric method. Dry samples, with a weight of 1.0 ± 0.1 g, were submerged in 50 mL of distilled water at room temperature, and the weight changes of the adsorbent were measured at an interval of time until equilibrium was achieved. The sorption kinetics were monitored by measuring the weight at specified time intervals, with each measurement conducted in triplicate, and the data obtained had standard deviations below 5%, ensuring precision. The water absorption capacity, f_1, was calculated using the following equation (Equation (5)):

$$f_1 = \frac{(M_t - M_1)}{M_1} \times 100\% \quad (5)$$

where M_t (g) is the weight of the sample after water absorption, and M_1 (g) is the weight of the dry sample at the initial stage.

To model the water absorption dynamics, the Gallagher–Corrigan model was used to fit the experimental data. The model delineates the water absorbency process into two distinct phases: A rapid initial absorption phase (stage I), followed by a slower diffusion phase (stage II). The model fitting accuracy was assessed using the coefficient of determination (R^2). Furthermore, the analytical balance used for weight measurements was calibrated before each experiment. The equation for the model is shown below (Equation (6)):

$$f_1 = (f_1)_B \left[1 - \exp\left(-k_{g,1} \cdot t\right)\right] + \left[(f_1)_{max} - (f_1)_B\right] \left[\frac{\exp\left(k_{g,2} \cdot (t - t_{max})\right)}{1 + \exp\left(k_{g,2} \cdot (t - t_{max})\right)}\right] \quad (6)$$

where, $(f_1)_B$ refers to the cumulative absorbency profile in Stage I; $K_{g,1}$ and $K_{g,2}$ refer to the absorbency factors for Stage I and Stage II, respectively; t represents the time at which water absorbency is measured; t_{max} represents the time at which the transition from Stage I to Stage II occurs; and $(f_1)_{max}$ is the maximum absorbency ratio during the process.

Supporting Information

Supporting Information is available from the Wiley Online Library or from the author.

Acknowledgements

The authors gratefully acknowledge the Environment and Conservation Fund (Hong Kong) for financial support (project account: ECWW23EG03).

Conflict of Interest

The authors declare no conflict of interest.

Data Availability Statement

The data that support the findings of this study are available from the corresponding author upon reasonable request.

Keywords

environmental remediation, hydrogel, heavy metal stabilization, phosphate removal, slow-release fertilizer

Received: April 23, 2025
Revised: June 15, 2025
Published online:

[1] M. B. Shakoor, Z.-L. Ye, S. Chen, *Sci. Total Environ.* **2021**, *779*, 146240.
[2] B. Wu, L. Fang, J. D. Fortner, X. Guan, I. M. C. Lo, *Water Res.* **2017**, *126*, 179.
[3] W. Zhang, W. Ma, Y. Ji, M. Fan, O. Oenema, F. Zhang, *Nutrient Cycling in Agroecosystems* **2008**, *80*, 131.
[4] B. N. Ribeiro, A. P. Coelho, J. R. de Souza, L. de Gissi, L. B. Lemos, *Revista Brasileira de Engenharia Agrícola e Ambiental* **2022**, *26*, 924.
[5] C. Zhang, A. Guisasola, J. A. Baeza, *Water Res.* **2022**, *212*, 118102.
[6] L. Chen, X. Zhao, B. Pan, W. Zhang, M. Hua, L. Lv, W. Zhang, *J. Hazard. Mater.* **2015**, *284*, 35.
[7] W. Buss, C. Wurzer, M. Bach, J. Heberling, T. Appel, H. Gerber, O. Mašek, *Journal of Environmental Management* **2022**, *314*, 115035.
[8] Q. Yin, B. Zhang, R. Wang, Z. Zhao, *Environ. Sci. Pollut. Res.* **2018**, *25*, 4320.
[9] S. Kizito, H. Luo, S. Wu, Z. Ajmal, T. Lv, R. Dong, *Journal of Environmental Management* **2017**, *201*, 260.
[10] L. Leng, Q. Xiong, L. Yang, H. Li, Y. Zhou, W. Zhang, S. Jiang, H. Li, H. Huang, *Sci. Total Environ.* **2021**, *763*, 144204.
[11] M. Kończak, M. Huber, *J. Cleaner Prod.* **2022**, *331*, 129994.
[12] M. Liu, R. Li, J. Wang, X. Liu, S. Li, W. Shen, *Sci. Total Environ.* **2022**, *814*, 152752.
[13] B. A. Mohamed, R. Ruan, M. Bilal, S. Periyasamy, M. K. Awasthi, N. Rajamohan, L. Leng, *Renewable Sustain. Energy Rev.* **2024**, *192*, 114168.
[14] S. K. Das, G. K. Ghosh, *Energy* **2022**, *242*, 122977.
[15] B. Peng, Q. Liu, X. Li, Z. Zhou, C. Wu, H. Zhang, *Fuel Process. Technol.* **2022**, *230*, 107211.
[16] B. Geissler, L. Hermann, M. C. Mew, G. Steiner, *Minerals* **2018**, *8*, 395.
[17] P. D. Johan, O. H. Ahmed, L. Omar, N. A. Hasbullah, *Agronomy* **2021**, *11*, 2010.
[18] M. R. Maghsoodi, L. Ghodszad, B. A. Lajayer, *Environmental Technology & Innovation* **2020**, *19*, 100869.
[19] B. Altamira-Algarra, J. Puigagut, J. W. Day, W. J. Mitsch, J. Vymazal, R. G. Hunter, J. García, *Ecological Engineering* **2022**, *177*, 106571.
[20] P. E., S. Sarkar, P. K. Maji, *J. Environ. Chem. Eng.* **2024**, *12*, 113211.
[21] M. Guo, M. Liu, F. Zhan, L. Wu, *Ind. Eng. Chem. Res.* **2005**, *44*, 4206.
[22] F. Guo, W. Liu, W. Chen, F. Wang, H. Zhang, X. Jiang, J. Gardy, *J.Environm. Management* **2024**, *352*, 119910.
[23] Q. Zhao, W. Guo, B. Wang, X. Zhang, J. Li, *Journal of Water Process Engineering* **2024**, *57*, 104708.
[24] Q. Yin, B. Zhang, R. Wang, Z. Zhao, *Environ. Sci. Pollut. Res.* **2017**, *24*, 26297.
[25] I. W. Almanassra, G. Mckay, V. Kochkodan, M. Ali Atieh, T. Al-Ansari, *Chem. Eng. J.* **2021**, *409*, 128211.
[26] R. A. Ramli, *Polym. Chem.* **2019**, *10*, 6073.
[27] B. Li, S. Ding, H. Fan, Y. Ren, *Materials* **2021**, *14*, 447.
[28] K. Phoungthong, T. Suwunwong, *Res. Chem. Intermed.* **2020**, *46*, 385.
[29] J. T. N. Knijnenburg, S. Suwanree, D. Macquarrie, P. Kasemsiri, K. Jetsrisuparb, *RSC Sustain.* **2025**, *3*, 1084.
[30] J. Chen, L. Li, *Operations Research Letters* **2023**, *51*, 408.
[31] B. Cichy, E. Kużdżał, H. Krztoń, *Journal of Environmental Management* **2019**, *232*, 421.
[32] Q. Feng, M. Chen, P. Wu, X. Zhang, S. Wang, Z. Yu, B. Wang, *Chem. Eng. J.* **2022**, *429*, 132166.
[33] C. Feng, S. Zhang, Y. Wang, G. Wang, X. Pan, Q. Zhong, X. Xu, L. Luo, L. Long, P. Yao, *Bioresour. Technol.* **2020**, *307*, 123231.
[34] D. Ai, H. Ma, Y. Meng, T. Wei, B. Wang, *Sci. Total Environ.* **2023**, *860*, 160502.
[35] Q. Cui, G. Jiao, J. Zheng, T. Wang, G. Wu, G. Li, *RSC Adv.* **2019**, *9*, 18641.
[36] A. Zhang, S. Fang, H. Xi, J. Huang, Y. Li, G. Ma, J. Zhang, *Front. Environ. Sci. Engineer.* **2023**, *17*, 120.
[37] Y. Wu, X. Li, Q. Yang, D. Wang, Q. Xu, F. Yao, F. Chen, Z. Tao, X. Huang, *J. Environ. Management* **2019**, *231*, 370.
[38] Y. Zhi, D. F. Call, K. D. Grieger, O. W. Duckworth, J. L. Jones, D. R. U. Knappe, *Water Res.* **2021**, *202*, 117399.
[39] S. Biswas, S. Sharma, H. Siddiqi, B. C. Meikap, T. K. Sen, M. Khiadani, *Water Air Soil Pollut* **2021**, *232*, 8.
[40] S. Biswas, R. K. Diwakar, I. D. Behera, B. C. Meikap, T. K. Sen, M. khiadani, *J. Environ. Chem. Eng.* **2020**, *8*, 104441.
[41] S. Biswas, S. Sharma, S. Mukherjee, B. C. Meikap, T. K. Sen, *Journal of Water Process Engineering* **2020**, *37*, 101406.
[42] S. M. Davoodi, S. K. Brar, R. Galvez-Cloutier, R. Martel, *Fuel* **2021**, *285*, 119191.
[43] Y. Zhang, Z. Zheng, M. A. H. Badsha, I. M. C. Lo, *Sep. Purif. Technol.* **2024**, *341*, 126835.
[44] M. Farajpourla, S. R. M. Rao, V. V. B. Rao, *IOSR J. Environ. Sci., Toxicology Food Technol.* **2013**, *6*, 01.
[45] Y. Yang, H. Zhu, X. Xu, L. Bao, Y. Wang, H. Lin, C. Zheng, *Microporous Mesoporous Mater.* **2021**, *324*, 111289.
[46] H. Cao, X. Wu, S. S. A. Syed-Hassan, S. Zhang, S. H. Mood, Y. J. Milan, M. Garcia-Perez, *Bioresour. Technol.* **2020**, *318*, 124063.
[47] A. Kaur, A. Ali, *ChemistrySelect* **2021**, *6*, 6102.
[48] L. Wang, J. Wang, Y. Wei, *Colloids Surf. A* **2021**, *622*, 126589.
[49] Z. Wen, J. Ke, J. Xu, S. Guo, Y. Zhang, R. Chen, *Chem. Eng. J.* **2018**, *343*, 416.
[50] P. Wu, J. Zhong, N. Liang, C. Li, Q. Cao, M. Zhao, Y. Li, M. Liao, C. Yu, *RSC Adv.* **2024**, *14*, 27449.
[51] J. Li, B. Li, H. Huang, X. Lv, N. Zhao, G. Guo, D. Zhang, *Sci. Total Environ.* **2019**, *687*, 460.
[52] X. Liu, F. Zhu, R. Zhang, L. Zhao, J. Qi, *Renewable Sustainable Energy Rev.* **2021**, *135*, 110260.
[53] J. A. Baig, T. G. Kazi, M. B. Arain, A. Q. Shah, R. A. Sarfraz, H. I. Afridi, G. A. Kandhro, M. K. Jamali, S. Khan, *J. Hazard. Mater.* **2009**, *167*, 745.
[54] M. Zhao, D. Wang, Z. Fan, J. Lu, Y. Li, Y. Zhang, M. Lv, M. Sun, W. Wang, *Gels* **2025**, *11*, 150.
[55] J. Hao, B. Li, J. Tan, Y. Zhang, X. Gu, S. Wang, Y. Deng, X. Zhang, J. Li, *Adv. Sci.* **2024**, *11*, 2307793.
[56] V. Nenov, H. Yemendzhiev, G. Peeva, in *Phosphorus in Soils and Plants* (Eds. N. A. Anjum, A. Masood, S. Umar, N. A. Khan), IntechOpen, **2023**, https://doi.org/10.5772/intechopen.107701.
[57] V. Masindi, S. Foteinis, *J. Environ. Chem. Eng.* **2021**, *9*, 106625.